Proceedings of the
Annual Stability Conference
Structural Stability Research Council
San Antonio, Texas, March 19-22, 2024

Analyzing the Buckling Behavior of Steel Angle Sections in Transmission Towers

Liya Li[1], Sanaz Chehrazad[2], Saeed Mohebbi[3], Alex Loignon[4], Marc Demers[5], Charles-Philippe Lamarche[6], Sébastien Langlois[7]

Abstract

The buckling of steel angle members under compression loading in transmission towers is a critical failure mode that potentially leads to global structural collapse during extreme climatic events. This study aims to analyze and understand the buckling behavior of angle members in lattice towers through experimental testing of a tower section, followed by numerical analyses. A sub-assemblage of self-supporting lattice steel transmission towers was fabricated and subjected to critical design loads using a 6-degree-of-freedom loading setup. The angle members were tested under realistic conditions within a real lattice tower section, accounting for semi-rigid eccentric connections. This paper focuses on studying the pre- and post-peak buckling behavior of angle members under compression loading in a lattice tower context. Precise initial geometrical imperfections of the specimens were measured using digital image correlation (DIC) techniques. These imperfections were applied in the numerical models. The measured load and displacement data measured during the experimental phase were used to develop and validate ABAQUS shell element models for numerical simulation purposes. The ABAQUS simulations provided valuable insights into the buckling behavior of the steel angle sections. This comprehensive approach ensured an accurate representation of the structural response and enabled a deeper understanding of the buckling phenomenon in the context of lattice towers.

1. Introduction

The primary mode of failure in lattice towers is often the global buckling of the main supporting legs. The leg members are generally intercepted by diagonal members, which affects their effective buckling length. Evaluating the buckling capacity of angle leg members in lattice towers presents challenges. This is due to the interconnected nature of the main legs and diagonal braces within structures. These components not only offer mutual end support, but also continuously interact throughout the entire loading process (Xie and Sun 2013). Angle sections, commonly used in steel transmission towers, are crucial for maintaining structural stability under various load conditions. Their widespread use can be attributed to their low manufacturing cost, ease of fabrication

[1] Assistant Professor, Université de Sherbrooke, liya.li@usherbrooke.ca
[2] PhD student, Université de Sherbrooke, sanaz.chehrazad@usherbrooke.ca
[3] Post-Doctoral Fellow, Université de Sherbrooke, saeed.mohebbi@usherbrooke.ca
[4] Research Professional, Université de Sherbrooke, alex.loignon@usherbrooke.ca
[5] Research Professional, Université de Sherbrooke, marc.demers@usherbrooke.ca
[6] Professor, Université de Sherbrooke, charles-philippe.lamarche@usherbrooke.ca
[7] Associate Professor, Université de Sherbrooke, sebastien.langlois@usherbrooke.ca

involving only the drilling of holes, and simplicity in assembly, making them a preferred choice for lattice towers. Understanding the buckling behavior of these angle members is crucial for the integrity of the towers. As illustrated in Fig. 1 (Wakabayashi and Nonaka 1965), the tower model clearly shows the buckling of compression members, underscoring the significance of such analyses in the design and safety of towers.

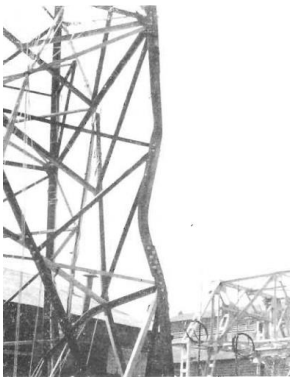

Figure 1: Buckling failure of angle in steel tower (Wakabayashi and Nonaka 1965)

Comprehensive research has been conducted on buckling in angle members, offering valuable insights into theoretical and practical perspectives. (Al-Sayed and Bjorhovde 1989) explored the buckling response of single angle columns, revealing a tendency for twisting and rotation during buckling and highlighting the influence of width-to-thickness ratios on failure load. (Huang *et al.* 2021) conducted an extensive study on equal-leg angle steel columns under compression, testing various specimens and comparing the results with four design standards, finding the standards generally conservative. (Dinis *et al.* 2012) proposed design procedures for fixed-ended and pin-ended equal-leg angle columns, emphasizing the differences in buckling responses and the need for specific design methods. Their Direct Strength Method (DSM) approach provided accurate strength estimates for columns over a broad slenderness range. (Sirqueira *et al.* 2020) investigated the behavior of carbon steel hot-rolled equal-leg angle columns under compression, noting significant discrepancies between Eurocode 3 (EC3 2005) compared to experimental and numerical results, thereby confirming the conservatism of these codes. (Shi *et al.* 2012) highlighted that local buckling in high-strength steel angles, especially in Q420 steel, cannot be ignored due to differing width-to-thickness ratios compared to ordinary steel.

In this study, a sub-assembly of a self-supporting lattice steel transmission tower was constructed and subjected to design load cases using a 6-degree-of-freedom loading system. This experimental setup replicated conditions akin to those in actual lattice tower structures, with a particular emphasis on identifying the angle members liable for global failure of the tower. To enhance the accuracy of the experimental phase, the specimens' initial geometrical imperfections were meticulously measured using advanced 3D scanners. Digital Image Correlation (DIC) techniques were employed to monitor and analyze deformation across the surface of the critical member. Concurrently, based on the applied loading history, a SAP2000 model (SAP2000 2003) was developed to determine the internal loads in the members composing the tower. ABAQUS shell element models, validated against existing experimental tests, were developed to investigate the buckling behavior of angle member columns with various end boundary conditions: pin-pin, pin-fixed, and fixed-fixed.

2. Experimental Program

This research involved testing a small-footprint self-supported latticed steel tower. The experimental test focused on the top two bays of the tower's tapered mast, just below the diaphragm marking the start of the tower head, as shown in Fig. 2. The tower consisted of L127×127×13 primary supporting legs and L51×51×4.8 diagonal braces. Table 1 summarizes the dimensions of these two types of angle sections - the width of angle leg b and the plate thickness t, as well as the average yield strength $F_{y,ave}$ and the average ultimate strength $F_{u,ave}$, obtained from the mill test.

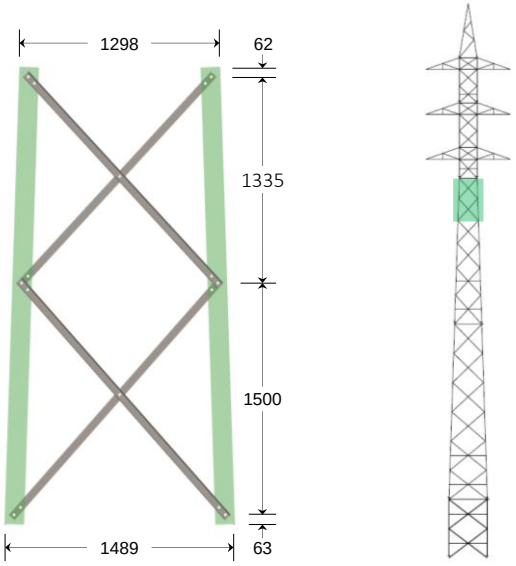

Figure 2: Dimensions of the tested specimen

Table 1: Angle sections selected

Angle membres	b (mm)	t (mm)	L (mm)	$F_{y,ave}$ (Mpa)	$F_{u,ave}$ (Mpa)
Primary leg members L127×127×13	127	12.7	2963.0	390	535
Diagonal braces L 51×51×4.8	50.8	4.76	1858.5 & 2042.5	358	464

The test specimens were tested in the Multi-Axis Structural Simulator (MASS), comprising a rigid cross, eight hydraulic actuators, and a 6-DoF (Degrees of Freedom) controller, as shown in Fig. 3. The vertical actuators can provide forces up to 1000 kN each for a total of 4000 kN, and the horizontal actuators, connected to reaction walls, had a 250 kN capacity each. The 6-DoF controller uses the initial geometry of the MASS, along with the force and movement of all actuators, to determine the displacements, rotations, forces, and torques on the specimen and control them as requested. Note that the horizontal actuators are rotated by 45 degrees respective to the longitudinal and transversal axis of the specimen. For specimen attachment, rigid steel plates were welded to the ends of the four primary support columns. These plates were subsequently bolted to a frame on the laboratory's strong floor at the bottom and connected to the MASS's rigid crossbeam at the top.

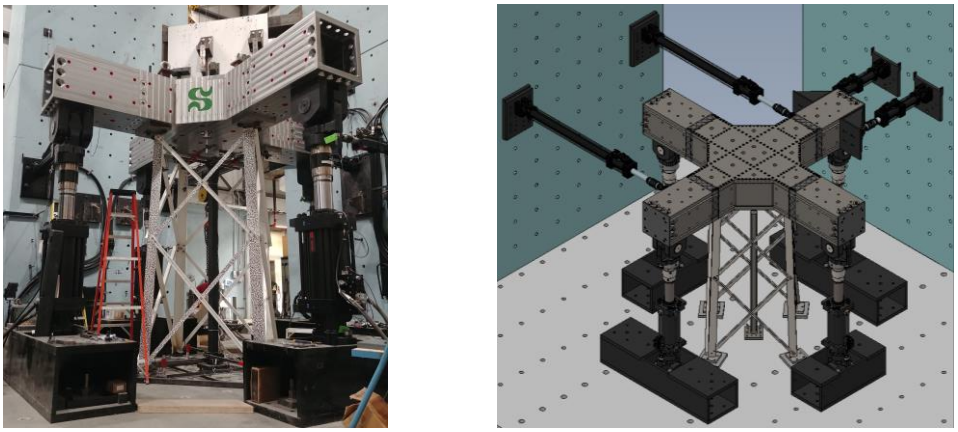

a) b)

Figure 3: Test setup – a) real setup in laboratory – b) 3d model of test equipment

This paper focuses on the heavy ice plus wind design load case, analyzing its impact on primary support columns until failure. Force control methodology was employed during the test, applying relevant force and torque to the rigid crossbeam. Table 2 details the loading control parameters used in this test as well as the test results when reaching ultimate resistance. During the test, the tower collapsed due to flexural buckling of one of the lower leg member, as illustrated in Fig. 5. Future analysis will concentrate specifically on this buckled angle member.

Table 2: Loading parameter and test results

	Loading rate (kN/min)	Design load (kN)	Test Results (kN)
Longitudinal translation F_x	2.77	-55.4	-135.7
Transversal translation F_y	3.47	-72.7	-173.5
Vertical translation F_z	18.31	-441.6	-972.6
	Loading rate (kN·m/min)	Design load (kN·m)	Test Results (kN·m)
Longitudinal rotation M_x	18.43	385.3	919.4
Transversal rotation M_y	21.08	-421.7	-1032.9
Vertical rotation M_z	0.00	0.0	-0.01

Additionally, two pairs of digital cameras were used for Digital Image Correlation (DIC), a non-contact optical tool used to measure deformation and strain on the surface of specimens. The accuracy of DIC is estimated to be between 0.015 mm and 0.030 mm. The objectives of employing DIC include: 1) measuring the initial imperfections of angle members, 2) tracking the movement of the specimen throughout the test, and 3) assessing the appearance of buckling at the critical angle section members. The distribution of the speckle pattern used for this analysis is illustrated in Fig. 4. The speckle pattern provides the required randomness and contrast to track the movements of every subset throughout the test.

DIC analysis results generated by using the VIC-3D tool (VIC-3D 2024) are presented in Fig. 5 et Table 3. The deformation ε of each column was calculated based on the displacement between two points located at the top and bottom of each member, i.e. Section (Sec) 1 to 4, as illustrated in Fig. 5a. During the test, it was observed that the deformation of each column increased to varying degrees, with the most significant deformation being observed in the buckling zone and at the diagonal brace connection of the most critical column (see white circles in c). The compressive loads N on each member or section is estimated using the formula $N = \varepsilon E A$, where ε represents

the strain, *E* is Young's modulus, and *A* is the cross-sectional area of the leg members. It is shown that when the tower system reaches its peak load, due to the buckling of the most critical column, the compressive load on this column is around 1242 kN.

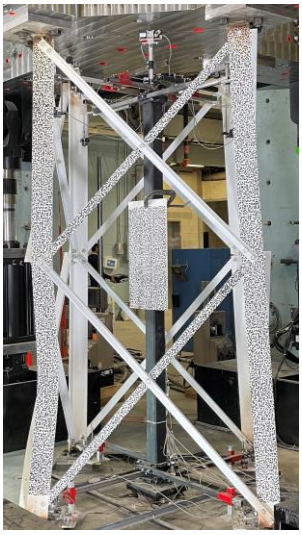

Figure 4: Distribution of the speckle pattern for DIC system

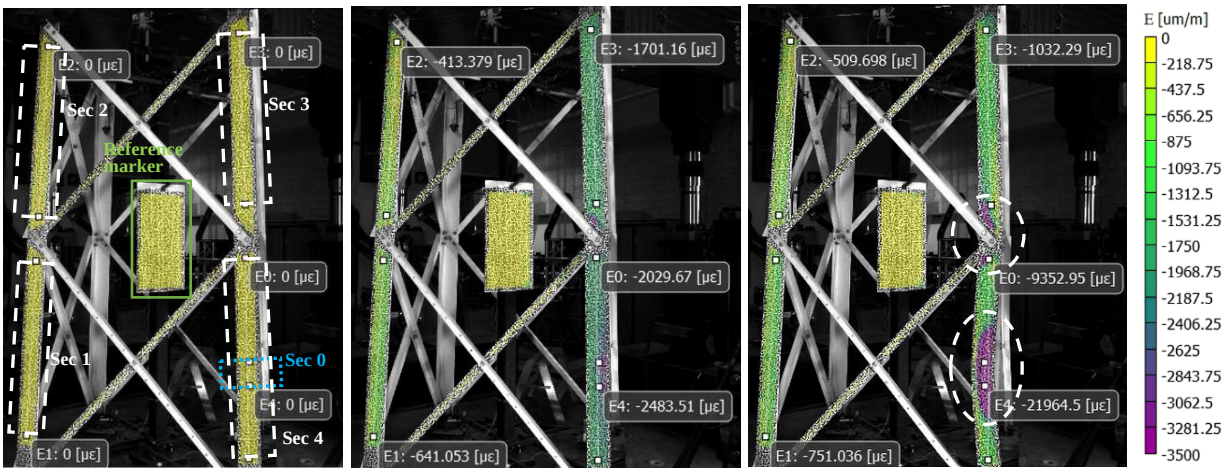

a) b) c)

Figure 5: DIC analysis results – a) initial status – b) peak load – c) post-load condition

Table 3: Strain distribution and estimated member load from DIC analysis

Status	Principal strain « E » (με)					Estimated member load (kN)				
	ε_1	ε_2	ε_3	ε_4	ε_0	N_1	N_2	N_3	N_4	N_0
initial	0.00	0.00	0.00	0.00	0.00	0.00	0.00	0.00	0.00	0.00
peak load	-641.05	-413.38	-1701.16	-2029.67	-2483.51	-392.32	-252.99	-1041.11	**-1242.16**	-1519.91
post-load	-751.04	-509.70	-1032.29	-9352.95	-21964.50	-459.63	-311.94	-631.76	-	-

The experiment was replicated using the SAP2000 software (SAP2000 2003). Both leg members and diagonal members were modeled as beam elements. Fig. 6 illustrates the boundary conditions and the application of loads in the SAP2000 model. Rotational and displacement constraints were fixed at the four start and end sections of the primary legs. Brace-to-leg connections were modeled as hinge connections, in accordance with the primary design assumption of the tower as a truss.

Linear material properties were considered for the members since the analysis targeted the level of load up to the peak load.

The Elastic Modulus for the steel material was defined as 200 GPa with a Poisson ratio of 0.3. Forces and torques were applied at the center of the rigid members on the top, consistent with the test procedure. The distribution of these loads across the structural members was thoroughly analyzed, and the results are presented in Fig. 7.

The analysis reveals that the most critically loaded column, primarily undergoing axial compression, also experiences small bending moments. These moments result from the moment frame action of the columns with a rigid crossbeam due to rotational constraints at the top and bottom of the columns. Considering that the lateral stiffness of these moment frames was significantly less than that of the braced frame, induced moments in the column had low values. The compressive load on the column is 1177 kN, closely aligning with the estimates obtained from the DIC results, showing less than a 5% difference.

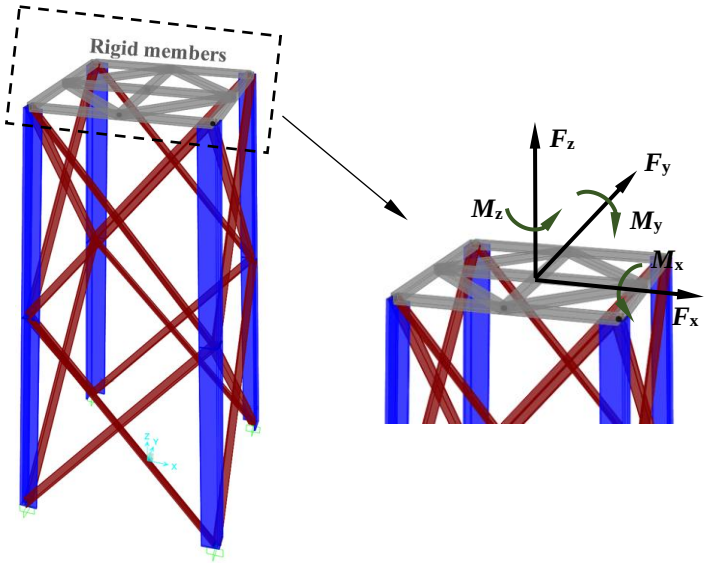

Boundary condition:
$U_x = U_y = U_z = 0$
$\theta_x = \theta_y = \theta_z = 0$

Figure 6: Boundary condition and loading application in SAP 2000 model

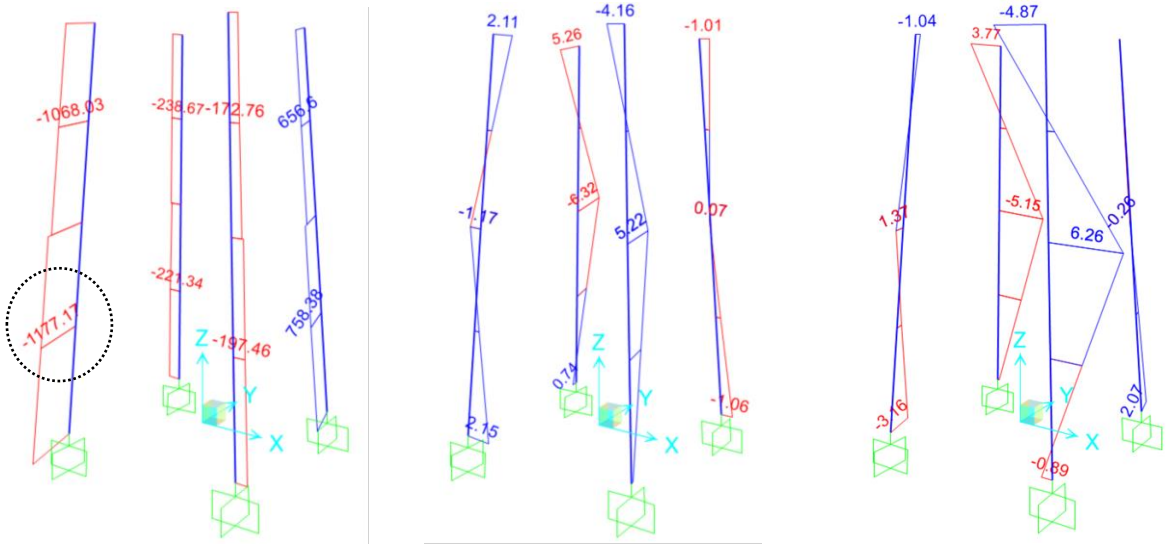

a) b) c)

Figure 7: Analysis results – a) Axial compression F_z – b) Bending moment M_x – c) Bending moment M_y

3. Numerical Analysis in ABAQUS

Detailed analysis of parts of the leg members were conducted using the non-linear finite element (FE) software ABAQUS. The S4R general-purpose shell element, frequently used in numerical studies on mono-symmetric and asymmetric sections (Liang *et al.* 2019; Li *et al.* 2022), was employed for the Geometrically and Materially Non-linear with Imperfections Analyses (GMNIA). To achieve an optimal balance between computation time and accuracy, the mesh size was chosen to be 1/15 × b. For both validation and further parametric studies in ABAQUS, a quad-linear stress-strain relationship (Yun and Gardner 2017), converted into true stress and logarithmic plastic strain, was utilized.

Three boundary conditions were considered: pin-pin, pin-fixed, and fixed-fixed, as shown in Fig. 8 and Table 4. For all conditions, both end sections were restrained against torsional rotation and against out-of-plane displacements about both principal axes, i.e., $U_y = U_z = \theta_x = 0$. At one end, the compression load was applied at a reference point which was coupled to the end section through rigid body conditions, while the longitudinal displacement U_x of the opposite reference point was prevented.

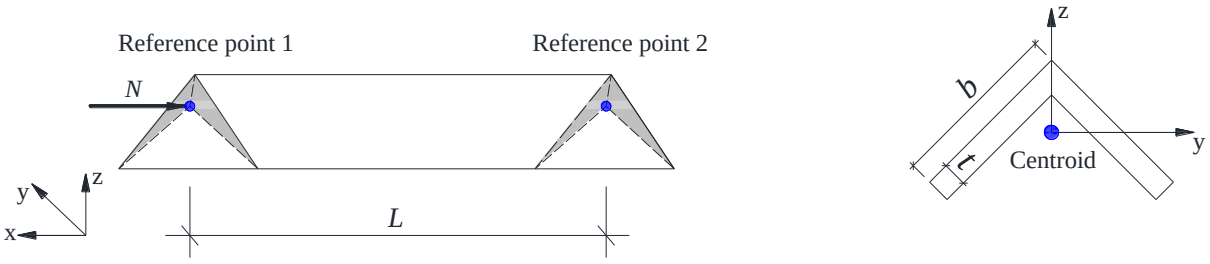

Figure 8: ABAQUS numerical models

Table 4: Boundary conditions in ABAQUS models

	Pin-Pin	Pin-Fixed	Fixed-Fixed
Reference point 1	$U_y = U_z = \theta_x = 0$	$U_y = U_z = \theta_x = 0$	$U_y = U_z = \theta_x = \theta_y = \theta_z = 0$
Reference point 2	$U_x = U_y = U_z = \theta_x = 0$	$U_x = U_y = U_z = \theta_x = \theta_y = \theta_z = 0$	$U_x = U_y = U_z = \theta_x = \theta_y = \theta_z = 0$

In the ABAQUS models, typical linear residual stress patterns were incorporated. Two distinct residual stress amplitudes, referred to as "Ampli", were analyzed, as illustrated in Fig. 9. Additionally, global geometrical imperfections were introduced into the FE shell models by altering node coordinates using sine-wave functions. Fig. 10 illustrates that the assumed half-wavelength for global buckling is L. The terms ω_{maj}, ω_{min} and θ represent the amplitudes of major-axis flexural, minor-axis flexural, and torsional global imperfections, respectively. To assess the sensitivity of angle member resistance to imperfection, three levels of amplitude were analyzed. These include ω_{maj} or ω_{min} equal to L/1000, L/2000, or L/3000, and θ calculated as $\tan^{-1}(L/1000/b)$, $\tan^{-1}(L/2000/b)$ and $\tan^{-1}(L/3000/b)$.

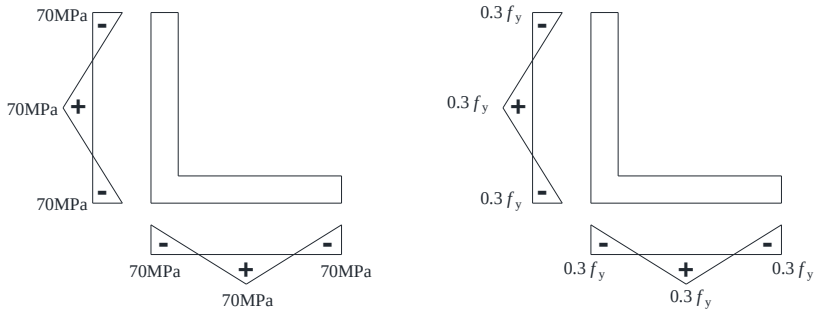

Figure 9: Definition of residual stresses – a) Type 1 with Ampli=70 MPa (Može *et al.* 2014) – b) Type 2 with Ampli=0.3f_y (ECCS 1976)

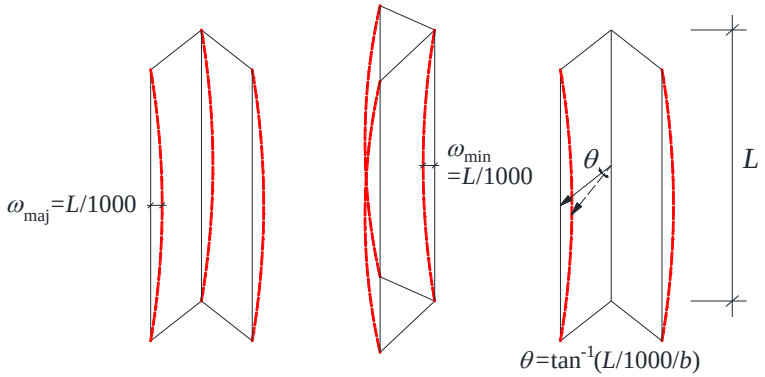

Figure 10: Definition of global geometrical imperfections

The FE models were firstly validated against experimental results reported by (Al-Sayed and Bjorhovde 1989) with pin-pin boundary condition, and then they were compared with the most critical leg members tested in the present study. For validation purposes, the numerical models incorporated measured dimensions of the specimens, including the widths of angle leg b, plate thickness t, effective column length L, and material properties such as yield strength f_y and ultimate strength f_u, as summarized in Table 5. The KL/r_y represents the slenderness ratio of columns, where r_y denotes the radius of gyration about the weak axis. The effective length factor K is set to 1 for these pin-pin columns.

Fig. 11 and Fig. 12 present a comparison between the experimental outcomes and numerical simulations for various residual stress patterns (see Fig. 9) and types of geometrical imperfection (see Fig. 10). These figures use the vertical axes to display normalized ratios of numerical ultimate capacity $N_{u,FE}$ to experimental ultimate capacity $N_{u,exp}$. A ratio of $N_{u,FE}/N_{u,exp}$ less than 1.0 indicates that numerical predictions are on the side of safety, and vice versa. Notable trends are observed:1) Members with Type 1 residual stress amplitude exhibit lower resistance, although the difference between Type 1 and Type 2 is marginal, less than 3%. 2) Member resistance shows higher sensitivity to minor-axis flexural global imperfections, particularly in short to medium length members. The disparity in resistance for members with ω_{min} equal to L/1000 and L/3000 can be as high as 20%. In contrast, major-axis flexural and torsional global imperfections have a negligible impact on the results. Ultimately, the combination of Type 1 residual stress pattern with ω_{maj} and ω_{min} set to L/1000, and θ calculated as $\tan^{-1}(L/1000/b)$ is selected for its closer alignment with the experimental findings. The numerical results using this combination are summarized in Table 5. The average $N_{u,FE}/N_{u,exp}$ ratio is 0.97, with a coefficient of variation (COV) of 0.04. It is concluded that the developed numerical models effectively predict the buckling resistance of angle members and are eligible to perform further studies.

Table 5: Section geometries, material properties and test results of leg members

Series	b (mm)	t (mm)	L (mm)	f_y (MPa)	f_u (Mpa)	KL / r_y (-)	$N_{u,exp}$ (KN)	$N_{u,FE}$ / $N_{u,exp}$ (-)
L1	76.20	9.53	736.17	321.79	530.71	49.40	418.75	0.95
L2	76.20	9.53	1538.95	321.79	530.71	103.27	230.51	0.92
L3	76.20	9.53	2329.22	321.79	530.71	156.30	103.77	0.99
L4	127.00	9.53	2040.88	309.10	495.54	81.18	501.38	1.00
L5	127.00	9.53	2812.43	309.10	495.54	111.87	320.40	1.00
L6	127.00	9.53	3891.70	309.10	495.54	154.80	178.53	1.01
L7	101.60	15.88	2233.33	296.21	423.08	112.84	428.09	0.91
L8	101.60	15.88	2969.39	296.21	423.08	150.03	232.56	1.01
							Mean	0.97
							COV	0.04
							Min	0.91
							Max	1.01

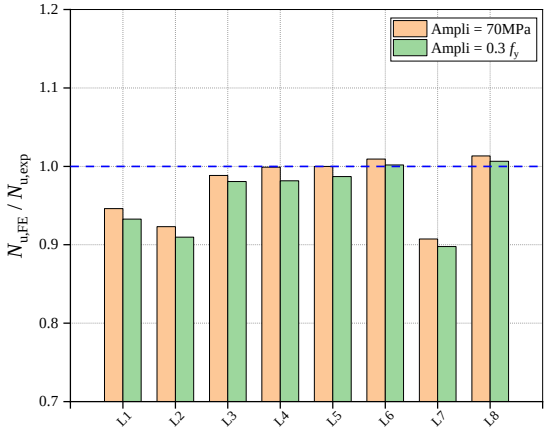

Figure 11: Comparison of test and numerical results with two types of residual stress amplitudes

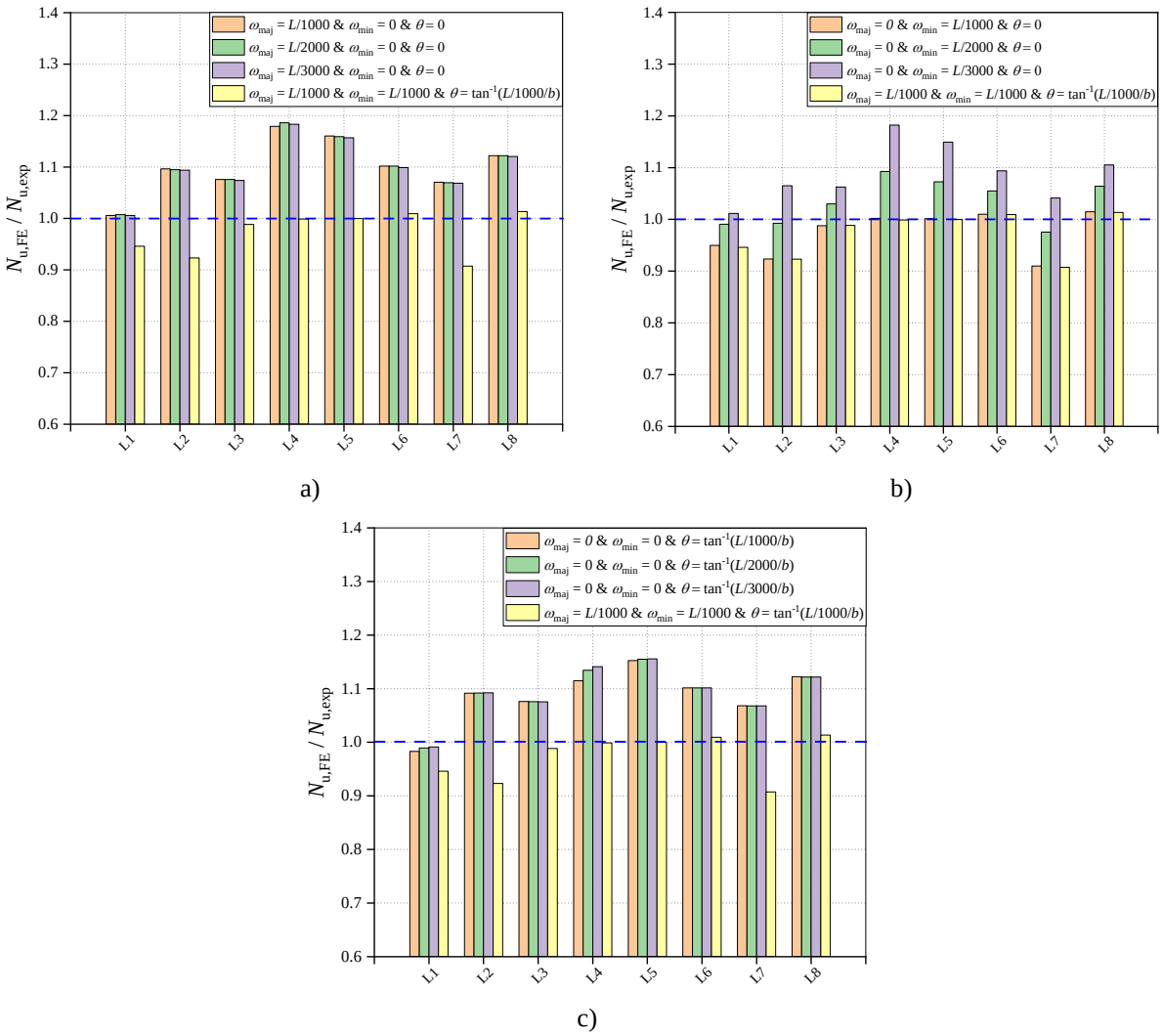

Figure 12: Comparison of test and FE results with various global geometrical imperfection types – a) major-axis flexural global imperfection – b) minor-axis flexural global imperfection – c) torsional global imperfections

The validated ABAQUS models were subsequently employed to analyze the most critical column identified in this research. Comparisons were made between the ABAQUS results and those obtained from the analysis of the results from the experimental test.

The study considered three types of boundary conditions: Pin-Pin, Pin-Fixed, and Fixed-Fixed ends. These findings are detailed in Table 6 combined with a comparison between the failure modes as shown in Fig. 13. The imperfection patterns scanned through DIC system were incorporated into the numerical models. These were then compared with the standardized imperfections identified in this study. Additionally, the results were evaluated against various standards, including the American (ASCE), Canadian (CSA), European (EC3) and the Australian (AS) steel design codes (ASCE 10-15 2015; CSA-S16 2019; EC3 2005; AS 4100 2020). It can be observed that: 1) the impact of bending moments, as shown in Fig. 7, on the ultimate resistance of legs is negligible; 2) the results using standardized imperfection patterns align closely with those employing scanned imperfection patterns, thereby validating the selection of imperfection

patterns; 3) the resistance predictions provided by all four design standards are consistently conservative except for the (ASCE 10-15 2015).

Table 6: Comparison between ABAQUS and experimental results

Assumed Boundary Condition	$N_{u,FE} / N_{u,Exp}$ (-)			$N_{u,ASCE} / N_{u,Exp}$ (-)	$N_{u,CSA} / N_{u,Exp}$ (-)	$N_{u,EC3} / N_{u,Exp}$ (-)	$N_{u,AS} / N_{u,Exp}$ (-)
	Scanned imperfection *N+M*	Scanned imperfection *N*	Standardized imperfection *N*				
Pin-Pin	0.80	0.82	0.84	0.83	0.72	0.72	0.66
Pin-Fixed	0.90	0.91	0.94	0.93	0.81	0.81	0.73
Fixed-Fixed	0.96	0.96	0.98	0.97	0.82	0.82	0.80

When examining the numerical models with pin-pin boundary conditions, it is evident from Table 6 that the results from ABAQUS tend to be overly conservative in comparison to test results. Conversely, the results yield more closely for numerical models with fixed-fixed and pin-fixed ends. Notably, the failure shapes observed in these configurations are similar. Among these, the pin-fixed end conditions are closest to those observed experimentally. As shown in Fig. 5c, large deformation at the connections with diagonal braces is observed, indicating a high likelihood of plastic hinge development in this area.

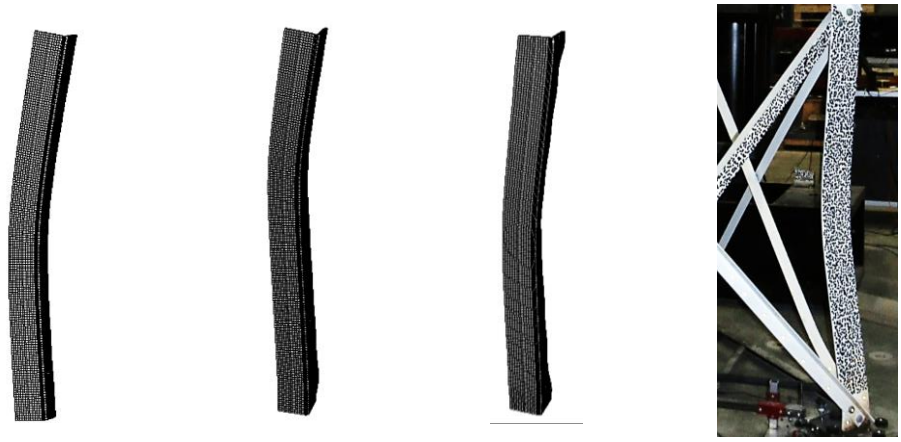

a) b) c) d)

Figure 13: Comparative analysis of failure modes in models with varied boundary conditions– a) pin-pin – b) pin-fixed – c) fixed-fixed– d) actual failure mode observed in experimental testing

4. Conclusions

This paper presents a comprehensive experimental and numerical analysis for the steel angle members typically used in power line transmission towers. A self-supporting lattice steel transmission tower sub-assemblies was tested under a 6-degree-of-freedom loading apparatus. This test used sophisticated DIC techniques to measure and analyze initial geometrical imperfections and deformation across the members, aiming to study the behavior of buckled angle members under compression loads. The experimental data is then used to develop and validate ABAQUS shell element models for further numerical simulations. The numerical simulations cover three boundary conditions – pin-pin, pin-fixed, and fixed-fixed – providing a deeper insight into the buckling behavior and a more profound understanding of the structural response of these steel angle members.

Acknowledgments

The test program was supported by the Natural Sciences and Engineering Research Council of Canada (NSERC), the InnovÉÉ funding program, the Fonds de recherche du Québec – Nature et technologies (FRQNT) through the strategic group CEISCE. The authors wish to thank the LabS platform at Université de Sherbrooke: Raphaël Prévost (technician), and Olivier Gauron (director), who participated to the testing program. Special thanks to Hydro-Québec for supplying the specimen drawings and corresponding load cases.

References

Al-Sayed, S.H. and Bjorhovde, R. (1989) 'Experimental study of single angle columns', *Journal of Constructional Steel Research*, 12(2), pp. 83–102.

AS 4100 (2020) *Steel structures*. Sydney: Standard Australia.

ASCE 10-15 (2015) *Design of latticed steel transmission structures*. American Society of Civil Engineers.

CSA-S16 (2019) *Design of Steel Structures*. CAN/CSA-S16:19. Canadian Standards Association (CSA), Mississauga, Ontario.

Dinis, P.B., Camotim, D. and Silvestre, N. (2012) 'Buckling, post-buckling, strength and design of angle columns', in *Structural Stability Research Council Annual Stability Conference*.

EC3 (2005) *EN 1993-1-1: Eurocode 3 - Design of steel structures - Part 1-1: General rules and rules for buildings*. European Committee for Standardization (CEN).

ECCS (1976) *Manual on Stability of Steel Structures*.

Huang, Z., Liu, H., Liu, H. and Li, Z. (2021) 'Experimental study on stability behavior of equal-leg angle steel columns', *Thin-Walled Structures*, 166, p. 108042.

Li, L., Gérard, L., Langlois, S. and Boissonnade, N. (2022) 'O.I.C.-based design of mono-symmetric I-sections under simple load cases', *Thin-Walled Structures*, 174, p. 109134.

Liang, Y., Jeyapragasam, V.V.K., Zhang, L. and Zhao, O. (2019) 'Flexural-torsional buckling behaviour of fixed-ended hot-rolled austenitic stainless steel equal-leg angle section columns', *Journal of Constructional Steel Research*, 154, pp. 43–54.

Može, P., Cajot, L.G., Sinur, F., Rejec, K. and Beg, D. (2014) 'Residual stress distribution of large steel equal leg angles', *Engineering Structures*, 71, pp. 35–47.

SAP2000 (2003) 'Analysis reference manual', *Computers and Structures, Inc., Berkley, California, USA*.

Shi, G., Liu, Z., Ban, H.Y., Zhang, Y., Shi, Y.J. and Wang, Y.Q. (2012) 'Tests and finite element analysis on the local buckling of 420 MPa steel equal angle columns under axial compression', *Steel & Composite structures*, 12(1), pp. 31–51.

Sirqueira, A.D.S., de Lima, L.R.O., Vellasco, P.D.S., Sarquis, F.R. and da Silva, A.T. (2020) 'Experimental and numerical assessments of hot-rolled carbon steel fixed-ended angles in compression', *Thin-Walled Structures*, 157, p. 107018.

VIC-3D (2024) *Correlated Solutions Digital Image Correlation*. Available at: https://www.correlatedsolutions.com/vic-3d.

Wakabayashi, M. and Nonaka, T. (1965) 'On the buckling strength of angles in transmission towers', *Bulletin of the Disaster Prevention Research Institute*, 15(2), pp. 1–18.

Xie, Q. and Sun, L. (2013) 'Experimental Study on the Mechanical Behavior and Failure Mechanism of a Latticed Steel Transmission Tower', *Journal of Structural Engineering*, 139(6), pp. 1009–1018.

Yun, X. and Gardner, L. (2017) 'Stress-strain curves for hot-rolled steels', *Journal of Constructional Steel Research*, 133, pp. 36–46.